



Support design in underground coal mines using modified rock mass classification system (RMR_{dyn}) for enhanced safety– an approach from stable and failed roof cases

Avinash Paul¹ · V. M. S. R. Murthy² · Amar Prakash¹ · Ajoy Kumar Singh¹

Received: 24 June 2023 / Accepted: 31 December 2023 / Published online: 25 January 2024
© The Author(s), under exclusive licence to Springer-Verlag GmbH Germany, part of Springer Nature 2024

Abstract

Bord and pillar method of mining continues to be a major operation in India with about 160 mines producing 35 MT of coal. Owing to the exhaustion of near-surface deposits, environmental impacts and land acquisition issues associated with surface mining, underground coal mining is expected to take a leap in the next decade. Weak and layered roof strata in underground mining play a significant role in roof failures in development headings affecting both safety and productivity. Despite well-defined support design guidelines based on CMRI-ISM RMR, roof failures are still a cause of great concern. In this research, firstly, a risk matrix has been framed on the basis of stable and unstable roof conditions for evaluating the potentiality of roof failure. This was followed by the development of a modified Rock Mass Classification System (RMR_{dyn}) considering Seismic velocity of rocks as one of the key parameters. A modified empirical relationship for rock load (RL) and a handy nomogram has been developed based on input parameters, namely, P-wave velocity, structural features, slake durability and groundwater condition. A guideline for roof support design has been framed based on rock load computed for RMR_{dyn} values ranging from 25 to 70. The developed models have been validated by statistical tools. The study also presents the risk classes to enable rock engineers to design more rational support systems in coal mine development headings.

Keywords Risk matrix · Dynamic rock mass classification system (RMR_{dyn}) · CMRI-ISM RMR · Rock load · Bord and pillar · Roof fall height (RFH) · Exposed bolt length (EBL)

Introduction

Coal mines in India are predominantly worked by bord and pillar mining method where a series of pillars are formed by driving roadways in both parallel and perpendicular direction (Singh et al. 2016). Out of the total coal production in India, 90% is worked by board and pillar mining and the rest 10% by the longwall mining method (Mukherjee and Pahari 2019). During the development of an underground mine, particularly in the layered strata, re-distribution of the stresses around the excavation causes deformation and sag

due to the new equilibrium of stresses achieved (Paul et al. 2012; Maazallahi and Majdi 2021). Lack of free face and blast-induced roof vibrations in blasting-off-solid have also a major effect in triggering the bed separation (Suresh and Murthy 2005; Xu et al. 2019). Thus, to retain the rock mass in its original state of equilibrium, mine roof should immediately be well supported soon after excavation is made since any excess time lag may cause the roof to deform (Kumar et al. 2019; Chen and Yin 2020). Roof fall in underground coal mines, especially in the freshly exposed roof, is always a matter of concern as it affects the safety and productivity of the workings (Agliardi 2003; Singh et al. 2005; Xu et al. 2019). Falls occur in all types of roof with a higher incidence in coal/shale roof rocks (Priest and Hudson 1976). Geological disturbances and structural anomalies have often triggered failure/roof failures if due care in support design is not exercised (Palmstrom 1982; Molinda 2003; Zhang et al. 2019). Roof falls are quite common in immediate weak strata (Esterhuizen and Bajpayee 2012) and they occur due to delayed and inadequate support (Ghosh and Ghose 1992;

✉ Avinash Paul
avinashpaul@cimfr.nic.in

¹ CSIR, Central Institute of Mining & Fuel Research, Dhanbad 826015, India

² Department of Mining Engineering, Indian Institute of Technology (Indian School of Mines), Dhanbad 826004, India

Zhao and Li 2021). Squeezing behavior of underground openings is experienced in deep workings due to overstraining which may require a special design in support (Dwivedi et al. 2014; Oge 2021).

Blasting in the development faces causes undesirable effects such as the heightening of the roof and also damages the rockmass around the opening (Saroglou et al. 2019). The damaged zone in coal mine development headings often makes the roof more vulnerable to failure with time as well as face advance (Mandal et al. 2008). Roof support is an important aspect of ground control during the development of the mine (Marinos and Hoek 2005; Prakash et al. 2018). The heterogeneity of the rocks, leading to uneven stress distributions around the underground excavation, requires a systematic approach in roof support design for long-term stability (Yan et al. 2020). The success of roof support reduces the incidence of roof falls as well as attributed to safer roof bolting practices (Paul et al. 2017). However, roof fall is still considered to be the number one occupational hazard contributing to 40–45% of the total fatalities in underground coal mines (Dash et al. 2016). Hence, a comprehensive roof characterization methodology is imperative for support design (Paul et al. 2018). For stability assessment of rock mass and design of the roof support system, it is necessary to estimate the magnitude of the rock load mobilised precisely (Laubscher 1993; Hoek et al. 1998). Thus, an appropriate rock load equation developed through the latest scientific tools is needed for rational and economic support design for underground coal mine development headings (see Fig. 1) (Paul et al. 2020a, b).

Study area

The collection of data from a large number of mines covering varied geo-mining conditions is essential to strengthening the objectives of the study. Field and laboratory investigations were carried out in seventy-nine coal mine sites covering four major coalfields, namely, Jharia coalfield (covering eight mine sites of Bharat Coking Coal Limited

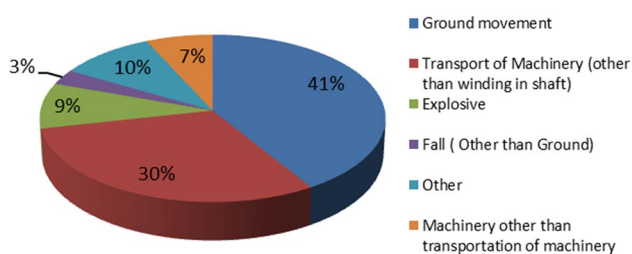


Fig. 1 Cause-wise accidents in underground coal mines of India (After Dash 2016)

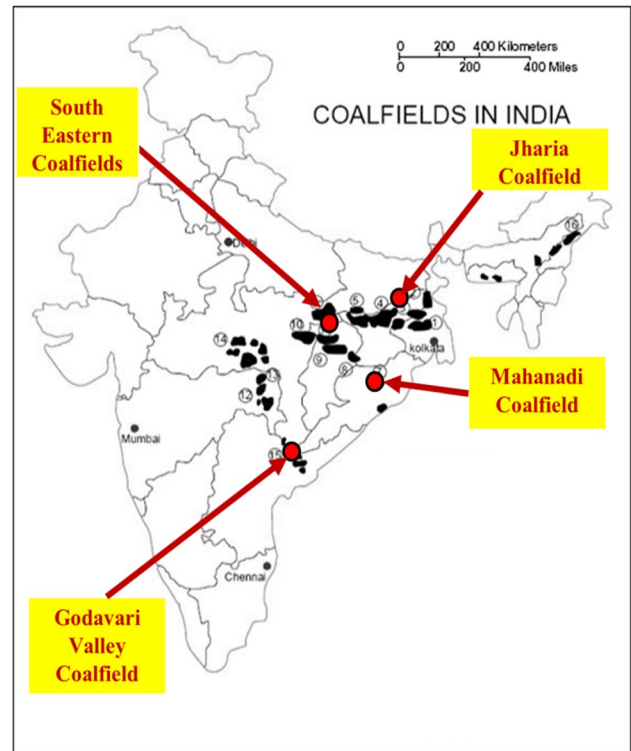


Fig. 2 Map of India showing different coalfields covered in the study (Dutta et al. 2011)

(BCCL) and Tata Steel Limited), IB Valley Coalfields (covering five mine sites of Mahanadi Coalfields Limited (MCL), Godavari Valley Coalfields (covering fourteen mines sites of Singareni Collieries Company Limited (SCCL)) and mines of South Eastern Coalfields Limited (SECL) (covering fifty two mines sites). The study locations are shown in Fig. 2.

Limitations of the present CMRI—ISM RMR system

In India, CMRI—ISM RMR classification is recommended for use in all the underground coal mines to evaluate the roof conditions (based on RMR) and designing suitable support system in development and depillaring headings (Paul et al. 2014). In this system, the rock load from the immediate roof is determined from an adjusted RMR value using an empirical equation developed (Venkateswarlu et al. 1987). The design of the support system is done for a given gallery dimension (B) and roof rock density (D) based on estimated rock loads using the empirical equation suggested. The same classification system has been used as a reference for investigating the cases under the current research. The basic parameters used in the CMRI—ISM

Table 1 CMRI–ISM RMR parameters and their rating

Parameter	Rating
Layer thickness (cm)	30
Structural features	25
Weatherability (%)	20
Compressive strength (kg/cm ²)	15
Groundwater (ml/min)	10

RMR are depicted in Table 1 and the rock load estimation equation is expressed as:

$$\text{Rock load in gallery (t/m}^2\text{)} = \text{B.D. [1.7 - 0.037} \\ \times \text{RMR + 0.0002} \times \text{RMR}^2\text{]} \tag{1}$$

For the 79 cases investigated, covering stable and failed, the causes for roof fall were analysed and it was found that the presence of bedding planes and joints in the immediate roof played a major role in the detachment of the roof. Blast-induced damage due to Blasting-off-solid, a predominant method of excavation in development headings, was also observed due to the use of higher charges in the blast holes, particularly, in the case of hard coals. Lack of free face in development headings is also another contributing factor for higher roof vibrations. Thus, initially, rock loads for development workings were determined with reference to the established CMRI-ISM RMR relation and accordingly roof failure cases were analysed as shown in Fig. 2. A good number of roof failure cases were observed for RMR values ranging from 30 to 45 possibly due to the under estimation of the rock load using CMRI-ISM RMR equation. No cases of roof failure were observed for RMR values above 50 which may be due to adequate or slightly over estimated rock loads.

Deviation in rock load could also be attributed to the arbitrary reduction of RMR by 10% for solid blasting cases,

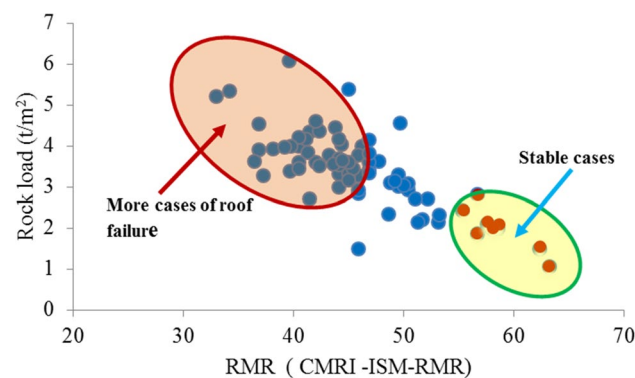


Fig. 3 Failure and stable cases observed in development headings

whereas the actual damage could be more or less due to the poor or good condition of the roof, respectively. With a few exceptions, the current rock load prediction equation holds good for RMR values ranging from 45 to 50 only. Thus, the relationship requires revision, especially, for low RMR values where the increasing occurrence of the roof fall has been noticed (see Fig. 3).

Risk matrix framework for roof failure

Analysis of the probability of roof failure is a strategic factor considering the unpredictability of its occurrence under similar rock mass condition. Probability of roof failure was computed for the 79 field cases (comprising of failed and stable roof conditions) under varied RMR and rock load categories. Roof failure and stable roof cases were segregated with respect to the RMR range as given in Table 2.

Sixty-two percent of roof failure cases were for an RMR value below 40 and they significantly decreased with increment in RMR value. The boundary condition of the rock load for roof failure analysis was outlined based on minimum and maximum rock density.

Analysis was done by abstracting established procedure of probability computation. Number of failure cases were considered as $P(A)$ and non-failure cases i.e., stable cases as $P(B)$ for probability analysis. Thus, the probability of the roof failure $P(F)$ would be the total number of roof failure cases divided by a total number of cases in that category. Similarly, for stable cases probability $P(S)$ was evaluated by considering the total number of stable cases divided by total number of cases falling under the respective category. The conceptual equations used for the determination of the probability of roof failure and stable cases are as follows (Ash 2008):

$$P(F) = \frac{P(A)}{P(A) + P(B)} \tag{2}$$

$$P(S) = \frac{P(B)}{P(A) + P(B)} \tag{3}$$

Table 2 Roof failure cases for different range of RMR

RMR range	Rock load range (t/m ²)	Failure cases	Stable cases	Total number of cases
30–40	5.3–4.0	18	10	28
40–50	3.45–3.01	10	15	25
50–60	2.94–2.03	1	15	16
60>	2.03–1.17	0	10	10

where, $P(F)$ is probability of failure cases, $P(S)$ is probability of stable cases. $P(A)$ is number of failure cases, $P(B)$ is number of stable cases.

Risk matrix is helpful in assessing the level of risk of roof failure by defining the consequence of the severity as it provides a good graphical projection of risk for different RMR ranges. It also helps in the identification of the areas where risk reduction has to be done. It also provides economic and quick risk analysis. It is a mechanism that increases risk visibility and helps the management in decision-making. Risk matrix was prepared based on four classes namely catastrophic, critical, marginal and negligible and categorized with respect to RMR and rock load values as shown in Fig. 4.

Catastrophic zone was demarcated as the most alarming zone where the RMR ranged from 30 to 40 and rock load varied from 4 to 5.3 t/m². The probability of roof failure ranged between 0.43 and 0.63. Similarly, a critical zone is a less severe zone compared to the catastrophic zone and the RMR and rock load values ranged from 40 to 50 and 3.01 to 3.45 t/m², respectively. The probability of roof fall in this zone is between 0.22 and 0.32 which is less than catastrophic zone. Likewise, the marginal zone was delineated as

the modest zone where the RMR value scaled from 50 to 60 with rock load variation from 2.03 to 2.94 t/m². In this zone, the probability of roof failure is between 0 and 0.21 which is very less compared to the catastrophic and critical zone. Negligible zone is defined for an RMR value greater than 60 (> 60) with zero roof failure probability. Thus, the class of the risk matrix is persuasive and significant in deciding emphasis on proper roof support measures and development of rational support design.

Determination of RMR_{dyn}

Considering the limitations of the CMRI-RMR Classification system, a new rock load equation was proposed for development headings based on additional investigations and some modified parameters. Dynamic RMR (hereinafter referred as RMR_{dyn}) was calculated for 31 mine sites from 79 investigated sites.

Determination of rock load

Actual rock loads were determined in 31 mine sites by three approaches, namely, roof fall height (RFH), exposed bolt length (EBL), and instrumentation (load cell) based on field conditions (Fig. 5).

RFH was measured and multiplied by the weighted density of the roof rocks to determine the rock load. This method was adopted at places of roof fall (Fig. 5a). Rock load was determined by measuring the length of the bolt exposed (EBL) after the fall of the roof or detachment of the immediate roof due to the presence of discontinuities or the presence of planes of weakness in the roof (Fig. 5b). The length of the exposed bolt was multiplied with the weighted density of the roof rocks present within the extent of fall. In the instrumentation method, a vibrating wire load cell was

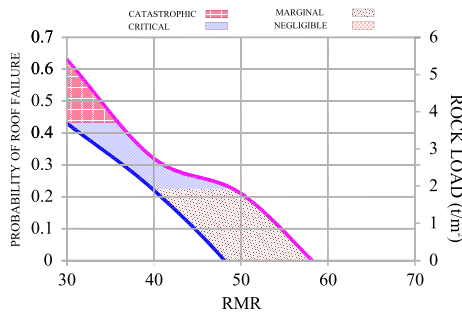


Fig. 4 Class of roof failure under varied RMR and rock load range

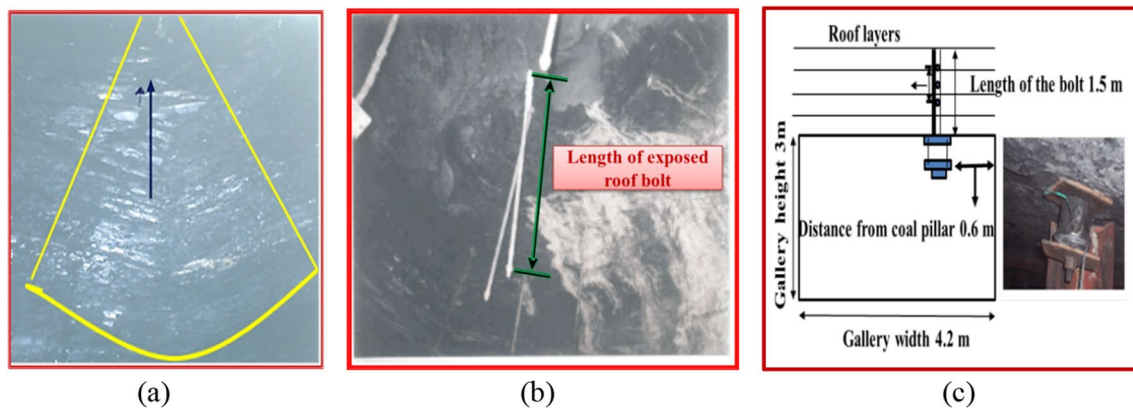


Fig. 5 Rock load estimation. **a** Loading arch with clear bending of roof (RFH method); **b** Exposed bolts due to detachment of layered beds (EBL method) **c** Installation of load cell in roof (Instrumentation)

used in a couple of selected mines to monitor the rock load. The typical installation methodology of the load cell in the mine roof is shown in Fig. 5c. The range of rock load varied from 1.1 t/m² to 6 t/m².

Determination of P-wave velocity using seismic refraction survey

The P-wave velocity (also known as compressional wave velocity), a new parameter, is included in the present study as it represents the competence of rock mass in-situ apart from *in-situ* layer thickness from the reflection coefficients (Scott et al. 1990; Hirata et al. 2000). The methodology for P-wave estimation is illustrated in Fig. 6.

Justification for inclusion of P-wave velocity

- i. *Influence of blasting*: The effect of blasting on roof damage was appropriately addressed by a few researchers only. Blasting engineers often resort to higher charges for obtaining higher pulls leading to elevated vibrations and roof damage. Therefore, an appropriate parameter that describes the competence of the roof in its entirety has an immense role in estimating the rock loads. Previous research carried out by Holmberg et al. (1978) and Murthy and Dey (2001) have demonstrated the impact of blasting in development headings and the care to be exercised in controlling the charges based on the threshold peak particle velocity of roof rocks. It is observed that the higher the P-wave velocity of the intact roof lesser will be the impact of blasting-off-solid (Murthy and Ray,

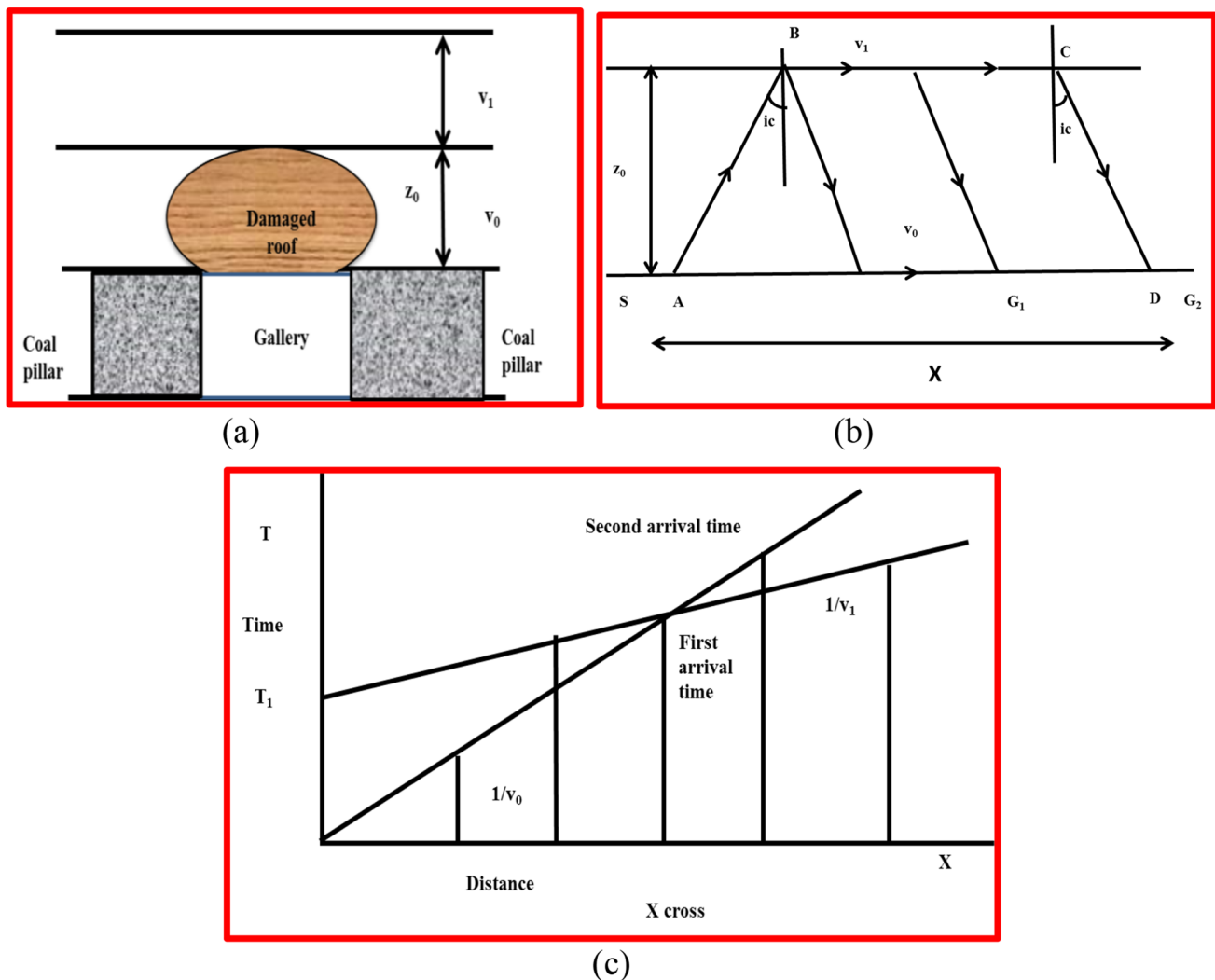


Fig. 6 Measurement of in-situ P wave velocity of roof rocks. **a** Sectional view of the damaged mine opening; **b** Refracted path of P-wave in two media case. **c** Time-distance graph in two media case (after Paul et al. 2020)

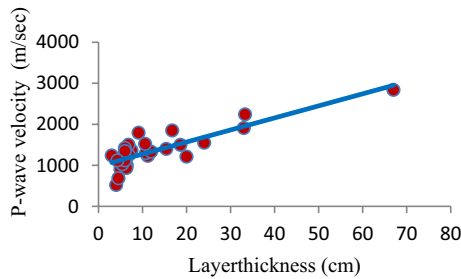


Fig. 7 Relation between Layer thickness and P-wave velocity

2002). Scientific investigations conducted by Murthy and Dey (2001) suggested optimum charges based on PPV, RMR, and P-wave velocity. The damage zones were also arrived at for different charge configurations through crater blast experiments (Murthy and Dey 2001). Thus, during the development of galleries, the roof rocks get damaged due to blasting-off-solid (characterised by lack of free face). Lower the competence of the roof in terms of RMR or P-wave velocity lower will be the allowable peak particle velocity (PPV) for limiting the damage zone. The arbitrary adjustment for blasting-off-solid in CMRI-ISM-RMR values, particularly in weak roofs, is a serious limitation that needs to be quantified. It may be summarized from the above discussion that P-wave velocity can be used as an indicator of roof competence as well as the resistance it can offer against blast-induced impacts.

- ii. *Rock mass condition*: Physical measurement of layer thickness is generally carried out through core drilling, exposing the roof by controlled blasting or by a recent roof fall case. In spite of the direct approach, practical constraints arise for determining the site-specific layer

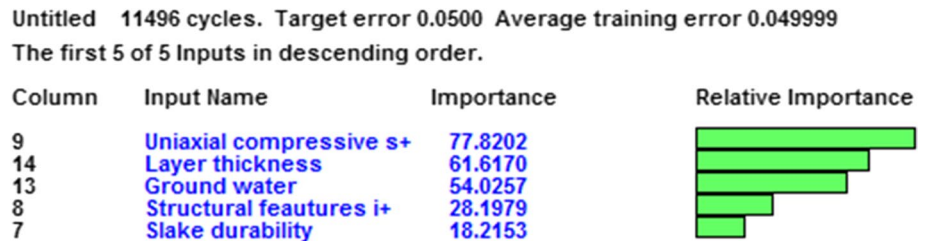
thickness in the case of unexposed roof sites. P-wave velocity is a representation of the cumulative influence of the structure, layer type in terms of its compactness as well as the thickness of the rock layer. An indirect approach of P-wave velocity determination to evaluate the rock mass condition will suffice the requirement without disturbing the unexposed roof. A correlation of layer thickness was also done with P-wave velocity with a good index of determination ($r^2 = 0.71$) (Fig. 7).

- iii. *Assumptions*: One of the assumptions is the 10% reduction in RMR accounting for the influence of solid blasting without any scientific basis. This is because the extent of the damage may be more or less based on the existing roof RMR/condition. Thus, this assumption can be eliminated by including P-wave velocity data.
- iv. *Uniaxial compressive strength (UCS)*: Intact rock gets deteriorated due to the high-intensity ground vibrations during blasting-off-solid during the course of gallery development. The insitu P-wave velocity takes into consideration the layering and blast-induced effects together. It reflects the competency of rock mass in a quantitative form. The *in-situ* P-wave velocity reflects the actual strength of the rock mass and hence UCS can be conveniently replaced by P-wave velocity.

Artificial neural network (ANN)

ANN technique was used to assess the dominant parameters influencing the P-wave velocity with respect to relative importance and relative sensitivity as shown in Figs. 8 and 9, respectively. Amongst the 31 cases investigated, layer thickness and UCS were observed to be the most dominant

Fig. 8 Relative importance of parameters influencing P-wave velocity



Untitled 11496 cycles. Target error 0.0500 Average training error 0.049999
The first 5 of 5 Inputs in descending order. Output column 12 P-wave

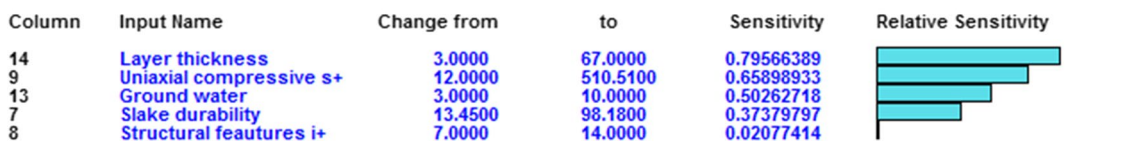


Fig. 9 Relative sensitivity of parameters influencing P-wave velocity

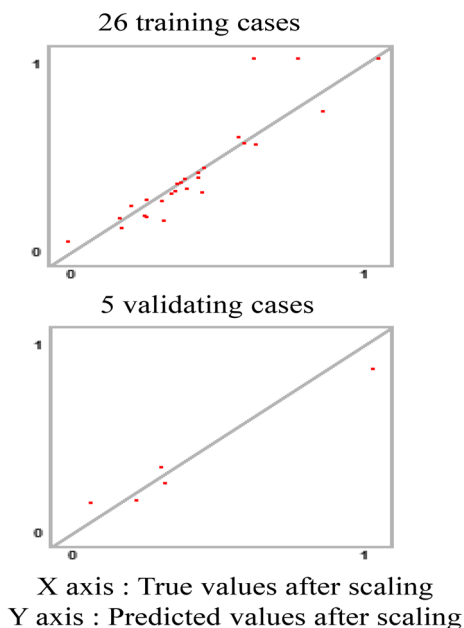


Fig. 10 Training and validation of the model

parameters. Both these represent the competence of roof and thus can be replaced by a single parameter, P-wave velocity.

This was further validated by predicting P-wave velocity using the back-propagation method with 5 random cases. It was found that the actual values were in close agreement with the predicted values of the trained model. The training and validation plots are shown in Fig. 10 (Shetty and Chellam 2003).

The data is scaled in both the axis between 0 to 1 in the process of training and validation. The predicted data shifts towards true value with a number of iterations and reach a state of saturation. The value of the target error can be from 0 to 0.9 but, if the value exceeds 0.2 then the network is said to be undertrained. For P-wave velocity prediction after 11,496 cycles, the value of target error was found to be 0.05, which is well within the maximum limit of 0.2. Thus, it may be concluded that the model is suitable for P-wave velocity prediction with reasonable accuracy.

Determination of P-wave velocity

Handy Viewer McSEIS-3 (MODEL-1817) was used for the determination of insitu P-wave velocity. The layout of instrumentation in underground development headings and determination of the P-wave velocity is shown in Fig. 11. Three geophones (G1, G2, and G3) are anchored in the roof at equal interval for receiving seismic waves. Z_0, Z_1 and Z_2 represent different layers in the roof and V_0, V_1 and V_2 are the corresponding seismic velocities. Seismic waves generated at point 'S' travel in hemispherical form and are received by the three geophones installed in the roof at a predetermined distances. (Paul et al. 2018).

Development of RMR_{dyn} classification system

As discussed, UCS and layer thickness in the existing CMRI-ISM RMR system were replaced by P-wave velocity. A new rating system is proposed after selecting and including the P-wave velocity as a parameter for developing a new RMR system here-in-after referred to as RMR_{dyn}, which ranged from 29.5 to 61.67 in the 31 cases investigated. The ratings of three parameters, i.e., structural features, slake durability and, groundwater were kept the same as that of the CMRI-ISM RMR system which summed up to 55 out of 100. The rating for P-wave was fixed as 45. A maximum P-wave velocity of 3500 m/s was observed during field investigations. However, the upper limit of the P-wave velocity of 4500 m/s was considered covering higher rock strength and in turn strong roof. The rating of the P-wave velocity may be determined from the following relation:

Table 3 Rating of P-wave velocity

P-wave velocity (m/s)	<1000	1000–2000	2000–3000	3000–4000	4000–4500
Rating	10	10–20	20–30	30–40	40–45

Fig. 11 Seismic imaging measurement technique

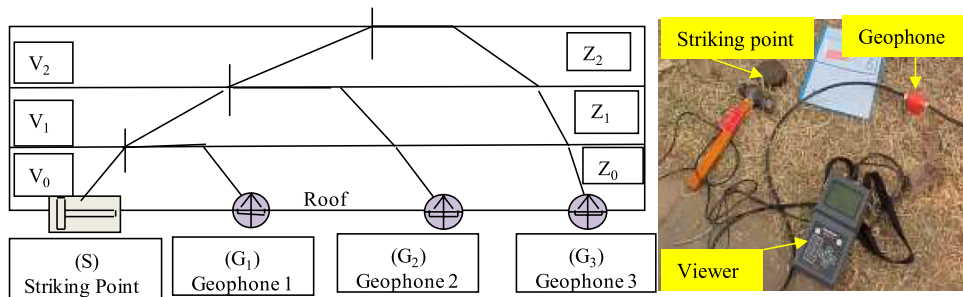


Table 4 Parameters of RMR_{dyn}

Parameter	Maximum rating
P-wave velocity (m/sec)	45
Structural features	25
Weatherability (1st cycle slake durability index)	20
Groundwater Condition (ml/min)	10

$$\text{Rating} = \text{Abs} \left[\frac{P - \text{wave}}{100} \right] \quad (4)$$

The rating of P-wave velocity was formulated based on Eq. (4), as given in Table 3.

RMR_{dyn} is determined considering four parameters, i.e., P-wave velocity, structural features, slake durability and, groundwater condition using the new rock mass rating system (Table 4).

RMR_{dyn} determined in 31 mine sites is detailed in Table 5. The maximum RMR_{dyn} of 61.67 (good roof condition) was found in KTK 6 mine, III seam main dip/3LS and a minimum of 29.5 (poor roof condition) in KTK 6 mine, I seam 13LN/BD.

Table 5 Investigated parameters for RMR_{dyn}

Mine sites	P-wave velocity (m/s)	Structural features indices	Slake durability (%)	Ground water (ml/min)	Density (t/m ³)	Width (m)	RMR _{dyn}
KTK 6 mine I seam II S.G. Rise	1907	7	47	3	2.08	3.6	40.5
KTK 6 mine I seam 13 LN/BD	1849	15	71.25	2	2.08	3.6	29.5
KTK 2 II seam	1497	10	90.4	8	2.3	3.6	46.2
KTK 6 II seam C dip/12LN	2240	13	94.4	10	2.17	3.6	52.2
KTK 6 III seam main dip/3LS	2838	7	91.3	7	2.18	3.6	61.67
VK Shaft King seam	1238	11	90.17	10	2.2	4.2	43
PVK 5 Shaft 6 King middle seam	1400	7	97.07	10	2.04	3.2	40
JK 5 Incline _35LS/39D	1211	14	95	10	1.5	4.2	49
JK 5 Incline _38LN/39D	1366	14	95	10	1.5	4.2	45
Bartaria LK II seam	1231	7	87.6	9	2.03	4.2	45
Jamuna 1/2 Incline	520	9	94.86	9	2.13	4.2	40
Bhadra 7/8 incline	1104	11	93.56	9	1.8	4.2	42
Jamuna 5/6 Incline	1550	8	62.62	8	1.82	4	42
JhilimiliV seam	910	11	95.83	8	1.4	3.8	40
Bijuri	1000	11	90.72	10	2.03	4.2	41
Kapildhara	1500	11	96.64	10	2.22	4.2	48
Rajnagar RO	1421	11	97.25	10	2.29	4.2	48
Haldibari	1298	9	13.45	9	1.67	4.8	35
Pinoura	1929	7	93.65	9	1.7	4.5	43.33
Nowrozabad	1333	11	82.74	9	1.9	4.2	40
Piparia	685	11	83.3	10	1.81	4.2	35.67
Rehar mine	2432	10	95.15	9	2	4.2	46.35
Vindhaya	935	11	86.83	9	1.62	4.2	38
Mine no 4 _24L/15DJ	1249	9.6	92.34	10	1.64	4.2	45.33
Mine no 4 _34L/5D	1523	11	89.26	10	1.94	4.2	45
Hirakhand Bundia A' section	1796	10	93.6	10	2.05	4.2	49
Hirakhand Bundia A section	1938	10	91.87	10	1.55	4.2	51
Bhelatand XIII seam	1022	11	97.16	8	1.31	4.2	37.8
Bhelatand XIV seam	1120	13	98.18	10	1.75	4.2	39.6
15 Pit Sijua XII seam	1347	12	97.61	8	1.82	4.2	39.48
8 Pit Sijua XII seam	1120	11	97.88	8	1.48	4.2	40.5

Table 6 Statistical parameters of RMR_{dyn}

Parameter	Minimum	Maximum	Mean	Std. Dev
RMR_{dyn}	29.50	61.67	43.3	5.94
Actual rock load (t/m^2)	1.10	6.00	3.80	1.21
Density(t/m^3)	1.31	2.30	1.88	0.27
Width of gallery (m)	3.20	4.80	4.08	0.31

Development of RMR_{dyn} -based Rock Load Model

The study conducted in different coalfields showed variations in RMR_{dyn} , the actual rock load, the density of rock, and the width of the gallery. The statistical details (minimum, maximum and mean) are given in Table 6.

The values of RMR_{dyn} ranged between 29.5 and 61.67 with a standard deviation of 5.94. 35% of the values of RMR_{dyn} ranged between 40 and 45 followed by 25% and 22% in the range of 35 & 40 and 45 & 50 respectively, as given in frequency distribution Table 7. An empirical relationship is developed for the determination of rock load using MATLAB tool by taking into account the gallery width and density of the rock, and expressed as:

$$RL (t/m^2) = B \times \gamma \times (31.85RMR_{dyn}^{-0.79} - 1.14) (R^2 = 0.95) \tag{5}$$

where RL is rock load (t/m^2), B gallery width (m) and γ is rock density (t/m^3).

Validation of the model

The developed rock load model was validated using statistical tools, i.e., T-test, ANOVA (analysis of variance) and residual analysis.

i. The t test

Table 8 The t test of various parameters for the developed equation

Parameters	t value	P-level
Rock load vs RMR_{dyn}	- 23.32	0.0000
Rock load vs density	9.64	0.0000
Rock load vs width	4.21	0.0002

The t test is generally used to compare the difference between two means with respect to its variation in data. The t test is also applied to determine the significance of the R values. The R values are said to be significant if the observations are taken on a random basis and the variables are distributed normally forming a bell-shaped distribution. The data is said to be statistically significant if the P value (level of significance %) is less than 0.05. The t test was conducted for RMR_{dyn} , the density of the rock and width of the gallery with respect to rock load and P-level was found to be less than 0.05 in each case as given in Table 8. Hence, it can be inferred that the data of all three parameters are statistically significant.

ii. ANOVA analysis

ANOVA is a statistical tool that is used to assess the variables having two or more categories. Generally, it is used for the assessment of the potential difference in a scale-level dependent variable through a nominal-level variable. In 1918, Ronald Fisher developed the ANOVA technique which is also called Fisher analysis. This technique eliminates the shortcomings of the t and z tests which only permit the nominal level variable to possess two categories.

The degree of freedom was 3 as three input parameters were taken and there were 31 cases. The statistical critical value at a 5% significance level of $F(3, 31)$ should be 2.91. The observed value of $F(3, 31)$ at a 5% significance level was 194.2 (Table 9).

Table 7 Frequency distribution of various parameters

RMR_{dyn}	Frequency	Gallery width (m)	Frequency	Actual rock load (t/m^2)	Frequency	Density (t/m^3)	Frequency
25–30	1	3.0–3.2	1	0–1	0	1.2–1.4	2
30–35	1	3.2–3.4	0	1–2	3	1.4–1.6	4
35–40	8	3.4–3.6	5	2–3	4	1.6–1.8	5
40–45	11	3.6–3.8	1	3–4	10	1.8–2.0	6
45–50	7	3.8–4.0	1	4–5	8	2.0–2.2	11
50–55	2	4.0–4.2	21	5–6	6	2.2–2.4	3
55–60	0	4.2–4.4	0				
60–65	1	4.4–4.6	1				
		4.6–4.8	1				

Table 9 Anova test of various parameters for the developed equation

Parameters	Sums of	df	Mean	F	p-level
Regression	55.60101	3	18.53367	194.2	0.000000
Residual	2.67194	31	0.09543		
Total	58.27295				

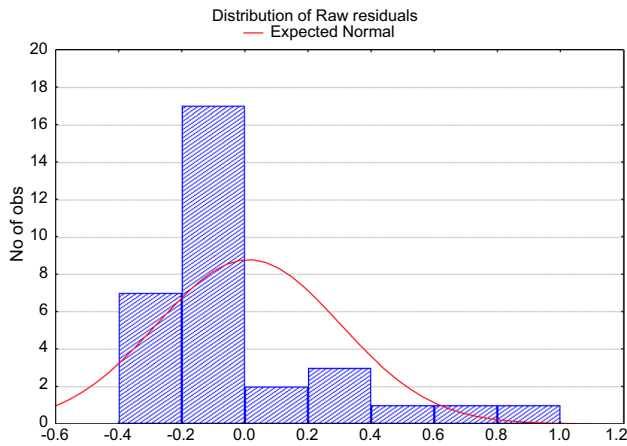


Fig. 12 Plot for residual analysis

This value was higher than the critical value. According to Cardinal and Aitken (2006), the observed value should be higher than the critical value. Hence, as per ANOVA analysis, the data were found to be statistically significant.

iii. Residual analysis

Sometimes the incorrect interpretation of the data can occur due to the presence of the extreme values which further lead to false conclusions. Thus, after fitting any regression equation, proper examination of the predicted and residuals are made. The validation of the model can be done by determining residuals. If the residuals are normally distributed with the zero mean and have constant variance, then the model is said to be a valid model (Goyal et al. 2006). Figure 12 shows the histogram plot of the residuals of the rock load model for the development galleries and the residuals were found to be distributed normally with the zero mean and constant variance.

Thus, the outcome of the *t*-test, ANOVA analysis, and residual analysis concluded that the newly developed rock load equation is significant and reliable and can be used for the rock load prediction for underground coal mine development headings.

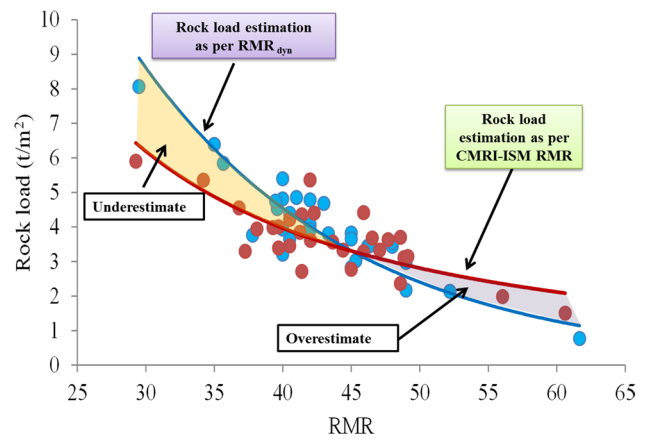


Fig. 13 Comparison of rock load with CMRI-ISM RMR and RMR_{dyn}

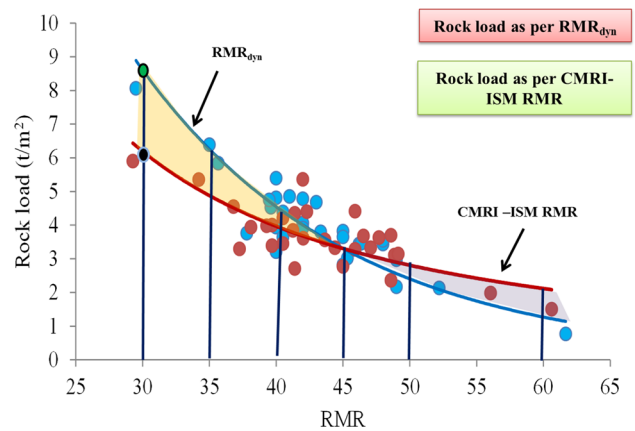


Fig. 14 Rock load variation with RMR_{dyn} in development headings

Comparisons of the rock loads

A comparison of the rock load was done for the CMRI-ISM RMR System and RMR_{dyn} as shown in Fig. 13. It was found that the rock load estimated by the CMRI-ISM RMR system was less for RMR value less than 45, in close proximity between 45 and 50, and overestimated above 50. Thus, it can be summarised that the CMRI-ISM RMR system does under prediction of the rock load for a low RMR range leading to inadequate support design thus causing the roof fall in investigated cases. The difference in the rock load, estimated by both systems, decreases with an increase in RMR up to 45 (RMR_{dyn} with higher values) followed by a trend reversal.

The deviation in rock loads increased inversely for RMR values beyond 45 (RMR_{dyn} with low values), as shown in Fig. 14. The difference in the rock load was quantified at different RMR to evaluate the actual deviation, as depicted in Table 10. The density and gallery width were kept as 2 t/

Table 10 Comparison of rock loads at different RMR range

RMR range	30	35	40	45	50	60
Rock load by RMR _{dyn} (t/m ²)	8.80	6.69	5.06	3.76	2.70	1.05
Rock load by CMRI-ISM RMR(t/m ²)	6.47	5.46	4.54	3.70	2.95	1.68
Difference in rock load (t/m ²)	2.33	1.23	0.52	0.06	-0.25	-0.63

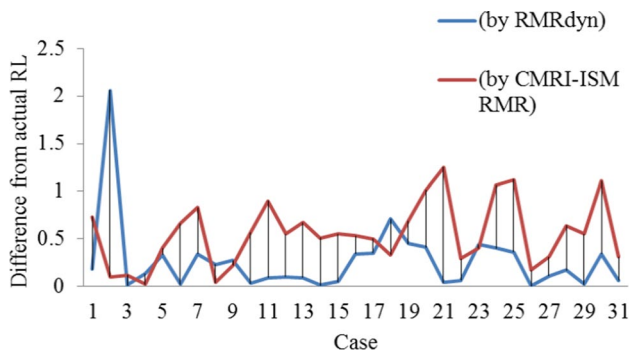


Fig. 15 Difference of rock loads using two approaches

m³ and 4.2 m, respectively, in both cases for the calculation of rock load as these values are most common in Indian mines. The difference in the rock load was as high as 2.33 t/m² at 30 RMR. Rock loads predicted using RMR_{dyn} were on the higher side. This difference gradually reduced to almost nil for RMR values of 45 and a reverse trend was observed beyond it.

Validation with actual rock loads

The rock load determined by both the RMR systems was validated with the actual rock load. With one exception, the maximum standard deviation in the rock load determined by RMR_{dyn} was 0.50 whereas it was 0.88 in the case of CMRI-ISM RMR. The corresponding average standard deviation was 0.19 and 0.39, respectively. Hence the rock load estimated by RMR_{dyn} was found to be in close agreement with the actual in comparison to the rock load obtained by CMRI-ISM RMR. The rock load deviation of each case with the actual is given in Fig. 15. The average standard deviation between actual rock loads with RMR_{dyn} was found to be 0.19. On the other hand, the same was observed as 0.39 in the case of CMRI-ISM RMR. This shows that there was more deviation in rock load predicted using the CMRI-ISM RMR system compared to RMR_{dyn} with actuals.

Development of nomogram for RMR_{dyn} and rock load

A handy nomogram was developed for the prediction of RMR_{dyn} and rock load based on input parameters, namely, P-wave velocity (m/s), structural features; slake durability (%), and groundwater condition (ml/min) as shown in Fig. 16. The roof condition is categorised based on RMR_{dyn} values. The ratings of all the individual parameters are summed up with respect to the actual values determined at the site. The cumulative rating represents RMR_{dyn}. The RMR_{dyn} was categorised into five sections ranging from < 30, 30–40, 40–50, 50–60, and > 60. The roof condition (very poor, poor, fair, good and, very good) was classified based on the values of RMR_{dyn} obtained. This helps in assessing the roof class which ranges from I to V. The rock load was normalized with respect to gallery width and density. This concept was used to avoid the overlapping of the data in different roof classes thus will make it easy to read the nomogram. The actual rock load was determined by multiplying the normalized rock load with density and gallery width. The normalised rock load (t/m²) was obtained as per the actual value of RMR_{dyn} using the following equation:

$$RL_n = (31.85 \times RMR_{dyn}^{-0.7867} - 1.146) \tag{6}$$

$$RL_a = RL_n \times \gamma \times B \tag{7}$$

where RL_n is normalised rock load (t/m²), RL_a is actual rock load (t/m²), γ is density (t/m³) and B is gallery width (m).

Roof failure risk assessment-based support design

The nature of the roof condition, roof class based on RMR_{dyn} and, the likely rock load are imperative to suggest a suitable roof support system. A guideline for the estimation of the rock load based on RMR_{dyn} was developed for Indian geo-mining conditions as shown in Fig. 17. The boundary of rock load was established by varying the RMR_{dyn} values taking extreme values (minimum and maximum) of density and the gallery width into account. The roof condition was categorized with respect to the RMR_{dyn} as shown in Fig. 17. The value of the maximum rock load ranged between 4.94 t/m² and 11.96 t/m² at the RMR_{dyn} value of 30. The roof

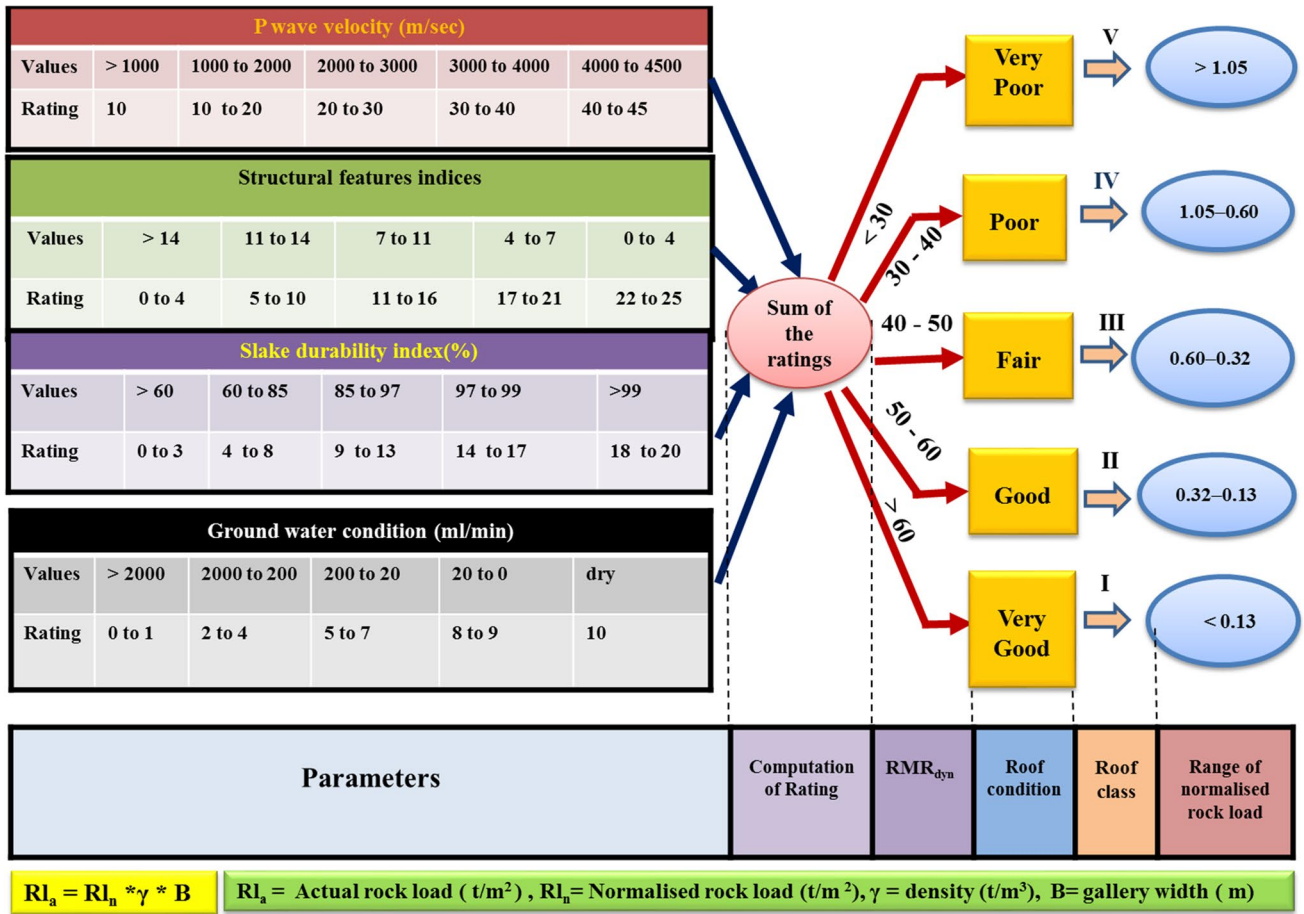
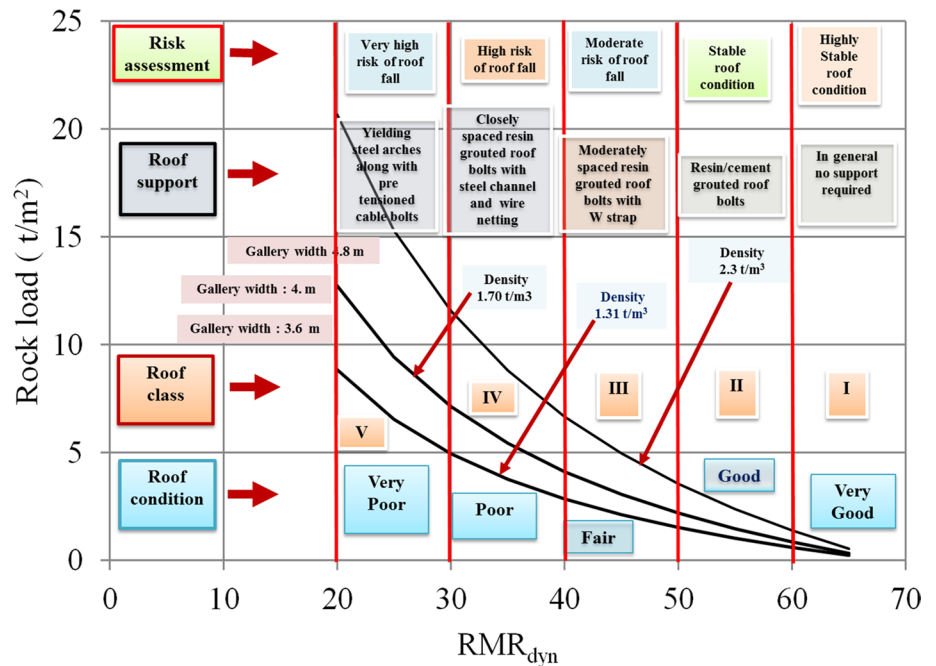


Fig. 16 Development of nomogram for RMR_{dyn} and Rock Load prediction

Fig. 17 Rock load estimation guidelines using RMR_{dyn}



condition and roof class were categorized as very poor and class V type for an RMR_{dyn} value of 30.



Under this condition, as a general guideline, the required roof support is yielding steel arch along with pre-tensioned cable bolts, if necessary, may be adopted. Such a region may be considered as a highly unstable zone with a very high risk of roof fall. Similarly, considering the RMR_{dyn} value as 40, the rock load values scaled from 2.84 t/m^2 to 6.66 t/m^2 . The roof condition and roof class fall in the poor category and class IV type respectively. The generalized support system should be closely spaced resin grouted roof bolts. This zone can be termed as an unstable zone with a high risk of roof fall. Likewise, when the RMR_{dyn} value is 50 the range of rock load will be between 2.19 t/m^2 and 3.55 t/m^2 . Here the roof condition can be characterized as fair and the roof class is type III. The support system applicable here can be moderately spaced resin/cement grouted roof bolts with W-strap. This zone can be said as a moderately unstable zone with a medium risk of roof fall.

When the RMR_{dyn} value is 60, the rock load values vary from 0.85 t/m^2 to 1.38 t/m^2 . Here the roof condition can be characterized as good and the roof class as type II. This zone can be said as a stable zone with minimal chances of roof fall unless affected by local geological disturbances. For the RMR_{dyn} value of 65, the maximum and minimum rock load values range between 0.32 t/

m^2 and 0.53 t/m^2 . Here the roof condition falls under the very good condition and termed as a highly stable zone and the type of roof can be stated as roof class type I. In a highly stable zone, in general, no support is required. However, the site-specific condition needs investigation to finalise the exact support. The variation in rock load for all the zones is primarily due to variation in density and gallery width. The above are some guidelines for roof support in such conditions. A site-specific and detailed investigation is, however, essential for designing and cross-checking the actual roof support.

A broad guideline for the support design was also outlined for RMR_{dyn} ranging from 25 to 70. Rock load was calculated for different densities and gallery width. A factor of safety (FOS) was fixed considering the roof class with FOS values decreasing from 2.2 to 1.5 with decrease in rock class. Support resistance, for various types of support commonly used such as arches, resin and cement-grouted roof bolts, was computed by multiplying the rock load with a factor of safety. Accordingly, support design for various gallery widths commonly practised in Indian geomining condition was done as depicted in Table 11.

Table 11 Broad support design guidelines

Class	RMR_{dyn}	Rock load (t/m^2)			FOS	Support resistance (t/m^2)			Support type	Support layout with gallery width				
		B	3.6	4		4.8	B	3.6		4	4.8	3.6 m gallery	4.0 m gallery	4.8 m gallery
		γ	1.3	1.7		2.3	γ	1.3		1.7	2.3			
V	25 - 30	6.5	9.4	15.3	2.2	143	21	34	Steel Arching	 Spacing : 1 m	 Spacing: 0.6 m	 Spacing :0.3 m		
IV	30 - 40	5	7	11	2.1	10.0	15	24	Resin bolts Bolt length : 2.1 m	 Number of bolts : 3 Bolt spacing: 1 m Row spacing: 1 m	 Number of bolts : 4 Bolt spacing: 1 m Row spacing: 0.8 m	 Number of bolts : 4 Bolt spacing: 1 m Row spacing: 0.4 m		
III	40 - 50	3	4	6.6	2.0	5.6	8	13	Resin bolts Bolt length : 1.8 m	 Number of bolts : 3 Bolt spacing: 1m Row spacing: 1.5 m	 Number of bolts : 4 Bolt spacing: 1 m Row spacing: 1.2m	 Number of bolts : 4 Bolt spacing: 1 m Row spacing: 0.6 m		
II	50 - 60	1.5	2	3.5	1.9	2.8	4.1	6.2	Cement grouted roof bolts Bolt length : 1.5 m	 Number of bolts : 3 Bolt spacing: 1 m Row spacing: 1.5 m	 Number of bolts : 4 Bolt spacing: 1 m Row spacing: 1.2 m	 Number of bolts : 4 Bolt spacing: 1 m Row spacing: 0.6 m		
I	60 - 70	0.5	0.8	1.3	1.5	0.8	1.3	2	No support	In general, no support required. Site-specific investigation is essential				

Note : B = Gallery width (m), γ = density (t/m^3)

Support specification

Steel Arches: Made of sigma steel, 60 Lb/m rails, load bearing capacity 50 tonne

Resin bolts: Bolt length 2.1 m, load bearing capacity 12 tonne*, dia should be 20-22mm, made of TMT/MS ribbed bar

Resin bolts: Bolt length 1.8 m, load bearing capacity 10 tonne*, dia should be 20-22mm, made of TMT/MS ribbed bar

Cement bolts: Bolt length 1.5 m, load bearing capacity 5 tonne*, dia should be 20-22mm, made of TMT/MS ribbed bar

Note : * Values based on field observation, # Rock load is calculated for lower values of RMR_{dyn} for each class

Conclusion

The limitations in the CMRI-ISM RMR system were outlined based on roof failure and stable cases investigated. It was observed that the maximum number of roof falls occurred in the low RMR range (< 45). The CMRI RMR ranging between 45 and 50 holds good support design. In other cases, it either underestimates or over estimates in the formulation of the support design. The importance and influence of the class of the risk matrix were noteworthy in highlighting the weightage of roof support measures and the development of rational support design. Layer thickness, structural features, slake durability, UCS and, groundwater conditions were measured to determine the CMRI-ISM RMR. Blasting in the underground mines affects the stability of the immediate roof in development headings mainly due to the lack of free face. Arbitrary assumption of a 10% reduction in RMR to account for the influence of BOS is the limitation of the CMRI-ISM-RMR system. P-wave velocity was included as a parameter by replacing layer thickness and UCS from the existing CMRI-ISM RMR system and a new rock mass classification system (RMR_{dyn}) was proposed. An empirical relationship was developed for the determination of rock load (RL) using RMR_{dyn} and validated by numerical modelling and statistical tools, i.e., t test, ANOVA (analysis of variance) and residual analysis. The developed model was observed to alleviate the limitations of the existing CMRI-ISM RMR system.

A handy nomogram was developed for the prediction of rock load based on input parameters, namely, P-wave velocity (m/s), structural features, slake durability (%) and, groundwater condition (ml/min) and was also validated with actual field conditions. The normalized rock load (RL_n) was computed as per the chart and the actual rock load (RL_a) was determined by multiplying this value with density (γ) and gallery width (B). Support design guidelines were framed and risk assessment was projected on the basis of severity of the roof fall. The parameters included for risk assessment were roof condition, roof class and, the roof support system. Rock load curves were made using the RMR_{dyn} -based rock load equation and the severity of the roof fall was evaluated for appropriate support design. In the light of combined analysis and field corroboration, the newly developed rock load relationship using RMR_{dyn} classification was found to be reliable and significant and could explain the gaps in the previous CMRI-ISM RMR. Thus, the developed rock load predictor equation can be used for the design of support system in coal mine development headings. More field cases can help fine-tune the developed approach.

Acknowledgements The authors are thankful to different coal mining companies, namely, BCCL, SECL, SCCL, and MCL for providing an opportunity to conduct the above-mentioned study. They were helpful during the preparation of the sites for study and sample collection which is highly appreciated. Authors would also like to thank Director, Indian Institute of Technology (Indian School of Mines) Dhanbad and Director, Central Institute of Mining and Fuel Research, Dhanbad for providing the required facilities for the completion of the study. This research forms a part of the doctoral thesis of the first author.

Author contributions AP: Manuscript writing, Field investigation, Laboratory investigations. VMSRM: Guided in data analysis. AP: Guided in data analysis. AKS: Guided in data analysis.

Funding Not applicable.

Availability of data and materials All data generated or analysed during this study are included in this article.

Declarations

Competing interests The authors declare no competing interests.

Conflict of interest On behalf of all authors, the corresponding author states that there is no conflict of interest.

Consent for publication The Authors hereby impart their consent for publication of their work in this esteemed journal. The paper covers a part of Ph.D. research work of the first author and the same has not been published nor sent anywhere for publication.

References

- Agliardi F, Crosta GB (2003) High resolution three-dimensional numerical modelling of rock falls. *Int J Rock Mech Min Sci* 40:455–471
- Ash RB (2008) Basic probability theory. Dover publication, New York, pp 10–14
- Cardinal RN, Aitken MRF (2006) ANOVA for the behavioural sciences researcher. Lawrence Erlbaum Associates, Mahwah
- Chen Q (2020) Yin T (2020) Modification of the rock mass rating system (RMR_{mbi}) considering three-dimensional rock block size. *Bull Eng Geol Environ* 79:789–810. <https://doi.org/10.1007/s10064-019-01596-x>
- Dash AK, Bhattacharjee RM, Aftab A (2016) Case study of accidents related to fall from height in Indian coal mining industry: an analysis. *Int J Sci Eng Res* 7:387–392
- Dutta P, Bhowmik S, Das S (2011) Methane and carbon dioxide sorption on a set of coals from India. *Int J Coal Geol* 85:289–299
- Dwivedi RD, Singh M, Viladkar MN, Goel RK (2014) Estimation of support pressure during tunneling through squeezing ground. *Eng Geol* 168:9–22
- Esterhuizen GS, Bajpayee TS (2012) Horizontal stress related failure in bedded mine roofs: Insight from field observations and numerical models. *Proceedings of the 46th U.S. Rock Mechanics/ Geomechanics Symposium*; Chicago, IL, Paper No. ARMA-2012. 137:68–77.
- Ghosh CN, Ghose AK (1992) Estimation of critical convergence and rock load in coal mine roadways – an approach based on rock mass rating. *Geotech Geol Eng* 10:185–202

- Goyal P, Chan AT, Jaiswal N (2006) Statistical models for prediction of respirable suspended particulate matter in urban cities. *Atmos Environ* 40:2068–2077
- Hirata A, Sasao H, Yamazoe M, Obara Y, Kaneko K (2000) Compact vertical seismic profiling system and its application in underground excavation. International Society for Rock mechanics and rock engineering. ISRM international symposium, Melbourne
- Hoek E, Marinos P, Benissi M (1998) Applicability of the geological strength index (GSI) classification for very weak and sheared rock masses. The case of the Athens schist formation. *Bull Eng Geol Environ* 57:151–160
- Holmberg R, Persson PA (1978) Swedish approach to contour blasting. Proc. of 4th conference on explosives and blasting techniques, SEE, New Orleans. 1–3:113–127.
- Kumar A, Waclawik P, Singh R, Ram S, Korbel J (2019) Performance of coal pillar in deeper cover: Field and simulation studies. *Int J Rock Mech Mining Sci* 113:322–332
- Laubacher DH (1993) Planning mass mining operations. In: Hudson JA (ed) *Comprehensive rock engineering*, vol 2. Pergamon Press Oxford, New York, Seoul, Tokyo, pp 547–583
- Maazallahi V, Majidi A (2021) Directional rock mass rating (DRMR) for anisotropic rockmass characterization. *Bull Eng Geol Environ* 80:4471–4499. <https://doi.org/10.1007/s10064-021-02143-3>
- Mandal PK, Singh R, Maiti J, Singh AK, Kumar R, Sinha A (2008) Underpinning based simultaneous extraction of contiguous sections of a thick coal seam under weak and laminated parting. *Int J Rock Mech Mining Sci* 45(1):11–28
- Marinos P, Hoek E (2005) The geological strength index: applications and limitations. *B Eng Geol Environ* 64:55–65
- Molinda GM (2003) *Geologic hazards and roof stability in coal mines*. Pittsburgh, PA: U.S. Department of Health and Human Services, Public Health Service, Centers for Disease Control and Prevention, National Institute for Occupational Safety and Health, DHHS (NIOSH) Publication No. 2003–152, IC 9466
- Mukherjee S, Hari P (2019) Underground and opencast coal mining methods in India: a comparative assessment. *Space Cult* 7:39–54
- Murthy VMSR, Dey K (2001) Roof damage prediction in solid blasting—an approach. *Minetech* 22:43–53
- Murthy VMSR, Ray SK (2002) Productivity optimization in weak sedimentary formations for improved coal production and roof stability—an approach. *Geotech Geol Eng* 20:273–290
- Oge FI (2021) Revisiting the assessment of squeezing condition and energy absorption of flexible supports: a mine development case. *Tunn Undergr Space Technol*. 8:103712. <https://doi.org/10.1016/j.tust.2020.103712>
- Palmstrom A (1982) The volumetric joint count—a useful and simple measure of the degree of the rock jointing. *Proc. 4th Congress. IAEG, Delhi* 5:221–228
- Paul A, Singh AP, John LP, Singh AK, Khandelwal M (2012) Validation of RMR-based support design using roof bolts by numerical modeling for underground coal mine of Monnet Ispat, Raigarh, India—a case study. *Arab J Geosci*. <https://doi.org/10.1007/s12517-011-0313-8>
- Paul A, Murthy VMSR, Singh AK (2014) Rock load estimation in development galleries and junctions for underground coal mines: a CMRI-ISM rock mass rating approach. *J Min*. <https://doi.org/10.1155/2014/618719>
- Paul A, Murthy VMSR, Prakash A, Singh AK (2017) Performance investigation of rock mass classification systems for coal mine support design in Indian mining conditions. *IJ e E* 10:1212–1219
- Paul A, Murthy VMSR, Prakash A, Singh AK (2018) Estimation of rock load in development workings of underground coal mines—A modified (RMR_{dyn}) approach. *Curr Sci* 114:2167–2174
- Paul A, Murthy VMSR, Prakash A, Singh AK (2020a) Estimation of rock load for junctions based on roof failure cases for safe mining operation. *Arab J Geosci*. <https://doi.org/10.1007/s12517-020-06045-8>
- Paul A, Murthy VMSR, Prakash A, Singh AK (2020b) Prediction of rock load emphasizing excavation damage of in-situ rock caused by blasting in coal mines. *Curr Sci* 118:123–132
- Prakash A, Kumar N, Kumbhakar D, Singh AK, Paul A (2018) A safe depillaring design for shallow depth of cover with influence of surface ground movements: a study in Jharia Coalfield. *Arab J of Geosci* 11(164):1–8. <https://doi.org/10.1007/s12517-018-3508-4>
- Priest SD, Hudson JA (1976) Discontinuity spacing in rock. *Int. J. Rock Mech Min Sci & Geomech Abstr* 13:135–148
- Saroglou C, Qi S, Guo S, Wu F (2019) ARMR, a new classification system for the rating of anisotropic rock masses. *Bull Eng Geol Environ* 78:3611–3626. <https://doi.org/10.1007/s10064-018-1369-9>
- Scott DF, Williams TJ, Denton DK, Friedel MJ (1990) Seismic tomography as a tool for measuring stress in mines. *Min Eng* 51:77–80
- Shetty GR, Chellam S (2003) Predicting membrane fouling during municipal drinking water nano filtration using artificial neural networks. *J Membr Sci* 217:69–86. [https://doi.org/10.1016/s0376-7388\(03\)00075-9](https://doi.org/10.1016/s0376-7388(03)00075-9)
- Singh AK, Paul A, Sinha A, Saikia K (2005) Geotechnical investigation for support design in depillaring panels in Indian coal mines. *J Sci Indus Res* 64:358–363
- Suresh R, Murthy VMSR (2005) Seismic Characterisation of Coalmine roof for rock load assessment. First Indian Mineral Congress, Dhanbad, Jharkhand, India, pp. 31–46
- Venkateswarlu V, Ghosh AK, Raju NM (1987) Rock mass classification for design of roof support—a statistical evaluation of parameters. *Min Sci Tech* 8:97–108
- Xu Y, Wu K, Li L, Zhou D, Hu Z (2019) Ground cracks development and characteristics of strata movement under fast excavation: a case study at Bulianta coal mine, China. *Bull Eng Geol Environ* 78:325–340. <https://doi.org/10.1007/s10064-017-1047-y>
- Yan H, Zhang J, Feng R, Wang W, Lan Y, Xu Z (2020) Surrounding rock failure analysis of retreating roadways and the control technique for extra-thick coal seams under fully-mechanized top caving and intensive mining conditions: a case study. *Tunn Undergr Space Technol*. <https://doi.org/10.1016/j.tust.2019.103241>
- Zhang C, Pu C, Cao R, Jiang T, Gang H (2019) The stability and roof-support optimization of roadways passing through unfavourable geological bodies using advanced detection and monitoring methods, among others, in the Sanmenxia Bauxite Mine in China's Henan Province. *Bull Eng Geol Environ* 78:5087–5099. <https://doi.org/10.1007/s10064-018-01439-1>
- Zhao X, Li Y (2021) Estimation of support requirement for a deep shaft at the Xincheng Goldmine, China. *Bull Eng Geol Environ* 80:6863–6876. <https://doi.org/10.1007/s10064-021-02350-y>

Publisher's Note Springer Nature remains neutral with regard to jurisdictional claims in published maps and institutional affiliations.

Springer Nature or its licensor (e.g. a society or other partner) holds exclusive rights to this article under a publishing agreement with the author(s) or other rightsholder(s); author self-archiving of the accepted manuscript version of this article is solely governed by the terms of such publishing agreement and applicable law.